Vol. 21, No. 3(2022) IA2879
Revista Mexicana de Ingeniería Química

Analytical and hybrid-neuro-differential approaches for describing contaminant removal from aqueous systems

Enfoques analítico e híbrido neuro-diferencial para la descripción de la remoción de contaminantes de sistemas acuosos

D. Temoltzin-Lobatón[1]*, K.H. Estévez-Sánchez[2], D. Cruz-González[1], C.E. Ochoa-Velasco[3], I.I. Ruiz-López[1]

[1]*Facultad de Ingeniería Química. Benemérita Universidad Autónoma de Puebla. Av. San Claudio y 18 Sur. Ciudad Universitaria. C.P. 72590. Puebla, Puebla. México.*

[2]*Facultad de Ciencias de la Electrónica. Benemérita Universidad Autónoma de Puebla. Av. San Claudio y 18 Sur. Ciudad Universitaria. C.P. 72590. Puebla, Puebla. México.*

[3]*Facultad de Ciencias Químicas. Benemérita Universidad Autónoma de Puebla. Av. San Claudio y 18 Sur. Ciudad Universitaria. C.P. 72590. Puebla, Puebla. México.*

Received: July 7, 2022; Accepted: September 2, 2022

Abstract

In this study, both analytical and hybrid-neuro-differential formulations were developed for describing the contaminant removal from wastewater by adsorption. The sorption isotherm, expressed as a straight-line equation (single segment or piecewise function) or artificial neural network (ANN), was coupled to the balance equations describing the pollutant transfer in adsorbent and wastewater phases, and their contact interface. The resulting wastewater adsorption remediation model (WARM) is valid for both batch and continuous operations, does not consider a dominant internal or external resistance to mass transfer or instantaneously equilibrated adsorbent, and has an analytical solution when a straight-line isotherm is used. The applicability of current model was tested in the analysis of two experimental datasets from literature describing the removal of the anionic dye direct red 23 (DR23) by graphene oxide (GO) and 4-nitrophenol (4NP) on calcium alginate-multiwall carbon nanotube beads (CAMCNB), where internal and external mass transfer coefficients and sorption isotherm parameters were simultaneously estimated by nonlinear regression. The analytical and hybrid-neuro-differential formulations were further compared with a numerical one where the WARM was coupled to Langmuir isotherm. Besides, the model was also used to explore different scenarios for continuous operation with all tested isotherms. It was demonstrated that the proposed formulations based on straight-line and ANN isotherms achieved a good reproduction of both dynamic and equilibrium experimental data, with similar fitness indices to that obtained with other non-linear equilibrium models.

Keywords: Analytical solution, Mass transfer, Pollutant, Wastewater.

Resumen

En este estudio se desarrollaron una formulación analítica y una híbrido neuro-diferencial para describir la remoción de contaminantes de aguas residuales por medio de adsorción. La isoterma de sorción, expresada como una ecuación de línea recta (de segmento único o definida por partes) o una red neuronal artificial (ANN), se integró en las ecuaciones de balance de masa que describen la transferencia del contaminante en las fases del adsorbente y agua residual, y en su interfaz de contacto. El modelo resultante de remediación de aguas residuales por adsorción (WARM) es válido para operaciones por lote y continua, no considera una resistencia externa o interna dominante a la transferencia de masa o un adsorbente equilibrado instantáneamente, y tiene solución analítica cuando se usa una isoterma de línea recta. La aplicabilidad del modelo propuesto se probó en el análisis de dos conjuntos de datos de literatura que describen la remoción del colorante aniónico rojo directo 23 (DR23) por óxido de grafeno (GO) y de 4-nitrofenol (4NP) por perlas de alginato de calcio-nanotubos de carbono multicapa (CAMCNB), donde los coeficientes interno y externo de transferencia de masa y los parámetros de la isoterma de sorción fueron estimados simultáneamente por regresión no lineal. Las formulaciones analítica e híbrido neuro-diferencial se compararon con una numérica donde el WARM se acopló a la isoterma de Langmuir. Además, el modelo se usó también para explorar diferentes escenarios de operación continua con todas las isotermas probadas. Se demostró que las formulaciones propuestas basadas en las isotermas de línea recta y ANN lograron una buena reproducción de los datos experimentales dinámicos y de equilibrio, con índices de ajuste similares a los obtenidos con otros modelos de equilibrio no lineales.

Palabras clave: Aguas residuales, Contaminante, Solución analítica, Transporte de masa.

* *Corresponding author. E-mail*: irving.ruiz@correo.buap.mx

https://doi.org/10.24275/rmiq/IA2879
ISSN:1665-2738, *issn-e*: 2395-8472

1 Introduction

Increasing water pollution by anthropogenic activities such as agriculture, mining, manufacturing, and urbanization has become a major concern in recent years (Wang *et al*., 2022). Major contaminants include different substances such as heavy metals, colorants, drugs, pesticides, and solvents, most of them of high toxicity to human health, able to cause endocrine dysfunction and immunological dysregulation, and with proven or suspected carcinogenic and mutagenic effects (Panis *et al*., 2022, Picetti *et al*., 2022).

Several technologies have been investigated for eliminating contaminants from wastewater such as photodegradation (Rueda-Márquez *et al*., 2020), cold plasma (Aggelopoulos, 2022), electrochemical oxidation (Qiao and Xiong, 2021), membrane distillation (Shirazi and Dumée, 2022), among others; however, the use of selective adsorber particles remains widespread because its relatively low cost, scale-up potential, excellent removal efficiency, high flexibility in operation, and no generation of additional pollutants (Zhang *et al*., 2021; Ahmed *et al*., 2022). Adsorbent materials can be chemically synthesized such as graphene oxide and nanostructured materials (Konicki *et al*., 2017; Zhang *et al*., 2021), isolated from natural sources such as zeolites, alginate, and chitosan (García-González *et al*., 2016; Ashrafi *et al*., 2021; Leo-Avelino *et al*., 2021), or obtained through functionalization of agricultural residues such as corncobes, plantain and prickly pear peels, oil palm bagasse, etc. (Villabona-Ortiz *et al*., 2020; Tejeda-Tovar *et al*., 2021a,b), further contributing to the sustainability of the adsorption process.

For batch operation, a dynamic mass transfer period originates in which pollutant is gained by the adsorbent when the last is immersed in the wastewater. The contaminant adsorption continues until it reaches a stationary state if the process is performed for a long enough time. Thus, the characterization of potential materials for wastewater remediation includes the evaluation of the maximum amount of removable contaminant, determined by the sorption isotherm of the adsorbent-pollutant system, as well as the speed at which adsorption occurs, determined by internal/external mass transfer coefficients or kinetics constants (Ayouch *et al*., 2020). Several alternatives are available for the mathematical description of the equilibrium stage, being the Langmuir, Freundlich, and Sips isotherms some of the most popular (Rangabhasyiyam *et al*., 2014; Ashrafi *et al*., 2021). The dynamic stage for mass transfer in batch operation is in turn described by models such as the first-order, second order and Elovich equations (Obón *et al*., 2022). These models assume that convection resistance is negligible for mass transfer, that is, the adsorbent surface instantaneously saturates (reaches its equilibrium concentration). For continuous operation, some models are available such as the Thomas, Yoon-Nelson, and Adams-Bohat equations for fixed bed adsorption columns (Chowdhury *et al*., 2013; González-López *et al*., 2021). These solutions are developed under specific assumptions; for example, Langmuir isotherm and second-order reversible reaction kinetics apply in Thomas model while surface reaction theory and non-instantaneous equilibrium are assumed in Adams-Bohat equation (Chowdhury *et al*., 2013). Still, they are only valid for a solid contained in the adsorption system with continuous feed of the liquid phase, a scenario not very suitable for the scale-up of some processes as the solid material could saturate quickly during operation (Verduzco-Navarro *et al*., 2020a), requiring adsorbent charge/discharge cycles and increased remediation times, whereas dynamic models exploring the continuous feed of adsorbent have yet to be reported.

Algebraic formulations are commonly favored when describing both the stationary and dynamic wastewater remediation processes very likely due to their simple and explicit nature. Nevertheless, ANN have recently attracted interest in the description of equilibrium and dynamic data for wastewater remediation processes due to their ability to manage highly complex systems where the use of traditional models may be flawed (Fagundez *et al*., 2021). In these cases, ANN are implemented in a direct form where they are used either to represent the sorption isotherm (Mendoza-Castillo *et al*., 2018) or to substitute a dynamic model (Chowdhury and Saha, 2013; Marzban *et al*., 2021). A major disadvantage of equilibrium and dynamic models, based on both traditional and ANN formulations, is that they are evaluated/fitted in an isolate manner. For example, dynamic models such as the first order kinetic equation contain the adsorption capacity at equilibrium (q_e), a term that could be evaluated from existing sorption isotherms; however, this parameter is very often estimated along the rate constant even if the sorption isotherm has already been determined (Konicki *et al*., 2017; Ayouch *et al*., 2020; Ashrafi *et al*., 2021). Thus, integral analyses where the sorption isotherm is included

and tested in the dynamic mass transfer model are required. The objective of this study was to develop a new approach for simultaneously describing both the stationary and dynamic adsorption stages during wastewater remediation. The approach is based on combining mass balances in liquid, solid, and liquid solid interface with both straight-line and ANN isotherms. The proposed model is valid for both batch and continuous operations, does not consider a dominant internal or external resistance to mass transfer or instantaneously equilibrated adsorbent, and has an analytical solution under the straight-line isotherm. The applicability of current model is further tested in the analysis of experimental adsorption data from literature.

2 Theory

Let us consider the removal of a single contaminant from water using an adsorbent material (solid phase) in an isothermal completely mixed system such as that presented in Figure 1. The following unsteady-state mass balances can be formulated in the liquid and solid phases:

$$\frac{dC}{dt} = -\frac{k_L A}{V_L}(C - C_i) + \frac{F_L}{V_L}(C_{in} - C) \tag{1}$$

$$\frac{dq}{dt} = -\frac{k_S A}{V_S}(q - q_i) + \frac{F_S}{V_S}(q_{in} - q) \tag{2}$$

where C is the mass of contaminant per unit volume of liquid phase, q is the mass of removed contaminant per unit mass of adsorbent, F is the volumetric flow rate, k is the mass transfer coefficient, A is the available surface for mass transfer, V is the volume, and the subscripts L, S, i, in denote the liquid phase, solid phase, solid-liquid interface, and inlet conditions, respectively. The mass flux of contaminant leaving the liquid phase should be equal to that transferred to the adsorbent, that is,

$$k_L(C - C_i) = k_S\rho(q_i - q) \tag{3}$$

where ρ is the apparent density of adsorbent. Besides, a sorption isotherm model, such as the Langmuir or Sips equations, is required to determine the mass equilibrium between the involved phases

$$q_i = f(C_i) \tag{4}$$

Eqs. (1) to (4) form a differential-algebraic system of equations hereafter referred as the wastewater adsorption remediation model (WARM) for simplicity. This system can be only numerically solved if the isotherm model is non-linear in nature; however, it may have an analytical solution if a linear isotherm model is used as demonstrated in the following sections. Mass balances in adsorbent, wastewater, and solid-liquid interface are expressed in terms of effective mass transfer coefficients and resemble other formulations used in fixed-bed solid-liquid adsorption (Hernández-Abreu *et al.*, 2020), fully mixed solid-gas adsorption (Thorpe, 2022), as well as other operations such as solid-liquid (Castillo-Santos *et al.*, 2010) and supercritical fluid liquid (Torres-Ramón *et al.*, 2021) extraction.

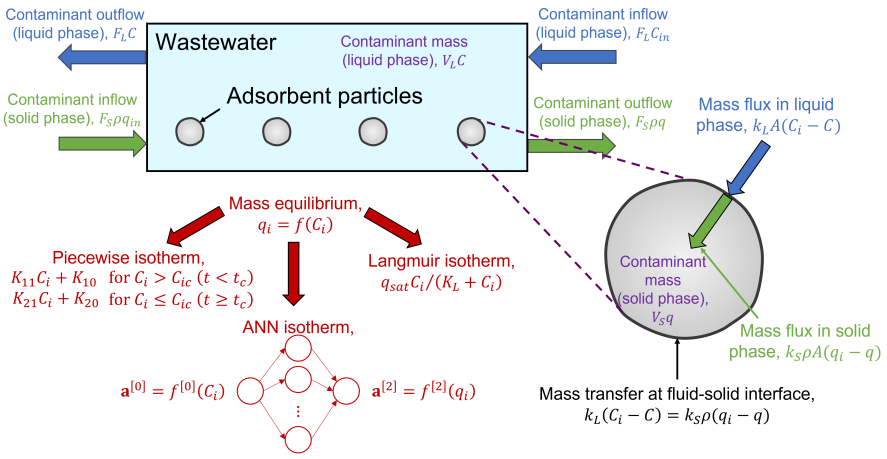

Figure 1. Schematic representation of adsorption system.

2.1 Analytical solution for batch operation

For batch operation $F_L = F_S = 0$. In this case, Eq. (1) is no longer needed as C and q are related by the mass balance

$$V_L(C_0 - C) = V_S \rho q = m_S q \tag{5}$$

where m is the adsorbent mass and the subscript 0 denotes the initial state. Eq. (5) considers negligible the initial amount of contaminant in the adsorbent. Let us consider a straight-line isotherm (SLI) having the form

$$q_i = K_{11} C_i + K_{10} \tag{6}$$

SLI models have been used in detailed numerical solutions of solid-gas adsorption (Thorpe, 2022) and extraction operations (Castillo-Santos *et al.*, 2010; Promraksa *et al.*, 2020). In addition, they have been also proven useful for obtaining analytical solutions describing the simultaneous heat and mass transfer between a moist solid and air during convective drying (Vargas-González *et al.*, 2021). An expression to evaluate C_i can be obtained by combining Eqs. (3), (5) and (6)

$$C_i = \frac{\left(k_S \rho - \frac{k_L m_S}{V_L}\right) q + k_L C_0 - K_{10} k_S \rho}{K_{11} k_S \rho + k_L} \tag{7}$$

The substitution of Eqs. (6) and (7) into Eq. (2) produces

$$\frac{dq}{dt} = \mathbf{A} q + \mathbf{B} \tag{8}$$

$$\mathbf{A} = -\frac{k_S A}{V_S}\left[1 + \frac{K_{11}}{K_{11} k_S \rho + k_L}\left(\frac{k_L m_S}{V_L} - k_S \rho\right)\right] \tag{9}$$

$$\mathbf{B} = \frac{k_S A}{V_S}\left[\frac{K_{11}}{K_{11} k_S \rho + k_L}(k_L C_0 - K_{10} k_S \rho) + K_{10}\right] \tag{10}$$

where parameters **A** and **B** contain the contributions of the state variable (q) and forcing function (a unit step) to the process dynamics. Eq. (8) can be analytically integrated between $t = t^*$, $q = q^*$ and $t = t$, $q = q_t$ to obtain

$$q_t = \frac{(\mathbf{A} q^* + \mathbf{B}) \exp[\mathbf{A}(t - t^*)]}{\mathbf{A}} - \frac{\mathbf{B}}{\mathbf{A}} \tag{11}$$

The subscript t has been added to q in Eq. (11) to explicitly indicate its value at a given time, while the superscript * denote a lower integral limit that is further defined as required (in this case, $t^* = 0$ and $q^* = 0$). The amount of removed contaminant by the adsorbent at any time can be calculated with Eqs. (9) to (11), while the remaining contaminant in bulk liquid (C) as well as interfacial concentrations in solid (q_i) and liquid (C_i) phases can be calculated from Eqs. (5), (6) and (7), respectively.

2.1.1 Piecewise linear isotherm

The description of mass equilibrium and adsorption kinetics can be improved by considering that the sorption isotherm can be approximated by a series of connected straight-line segments. This approach has been previously used to approximate the complex behavior of water sorption isotherm in drying models (Vargas-González *et al.*, 2021). For two segments, the following piecewise linear model is obtained

$$q_i = \begin{cases} K_{11} C_i + K_{10}, \text{ for } C_i > C_{ic} (t < t_c) \\ K_{21} C_i + K_{20}, \text{ for } C_i \leq C_{ic} (t \geq t_c) \end{cases} \tag{12}$$

Where C_{ic} represents the interfacial contaminant concentration in the liquid phase at the intersection of the straight lines and t_c is the time where it occurs, respectively. The intersection point coordinates are

$$(C_{ic}, q_{ic}) = \left(\frac{K_{20} - K_{10}}{K_{11} - K_{21}}, \frac{K_{20} K_{11} - K_{10} K_{21}}{K_{11} - K_{21}}\right) \tag{13}$$

The contaminant content in the bulk solid at the intersection (q_{tc}) can be calculated from Eq. (7) as

$$q_{tc} = \frac{(K_{11} k_S \rho + k_L) C_{ic} + K_{10} k_S \rho - k_L C_0}{k_S \rho - \frac{k_L m_S}{V_L}} \tag{14}$$

The value of t_c can be estimated from Eqs. (9), (10) and (11) once q_{tc} is determined

$$t_c = \frac{1}{\mathbf{A}} \ln\left(\frac{\mathbf{A} q_{tc} + \mathbf{B}}{\mathbf{A} q^* + \mathbf{B}}\right) + t^* \tag{15}$$

with $t^* = 0$ and $q^* = 0$. If the term within the logarithm is negative, then there is no need of changing from the first isotherm segment during simulation. The solution for the second stage is obtained by setting $K_{11} = K_{21}$, $K_{10} = K_{20}$, $t^* = t_c$ and $q^* = q_{tc}$ in Eqs. (6), (7), (9), (10) and (11). This procedure can be repeated to add more than two segments if needed.

2.1.2 Negligible external resistance to mass transfer

This case occurs when $k_L \gg k_S$; as a result, there is no concentration gradient in the liquid phase

and the adsorbent surface instantaneously reaches its equilibrium value ($C = C_i$, $q_i = K_{11}C + K_{10}$). The final solution is identical to Eq. (11) with $t^* = 0$ and $q^* = 0$, while new expressions for **A** and **B** are developed by taking their limit as $k_L \to \infty$. Thus, **A** and **B** become

$$\mathbf{A} = -\frac{k_S A}{V_S}\left(1 + \frac{K_{11} m_S}{V_L}\right) \tag{16}$$

$$\mathbf{B} = \frac{k_S A}{V_S}(K_{11} C_0 + K_{10}) \tag{17}$$

2.1.3 Negligible internal resistance to mass transfer

This case occurs when $k_S \gg k_L$; as a result, there is no concentration gradient in the adsorbent ($q = q_i$, $q = K_{11}C_i + K_{10}$). The final solution is now obtained for the bulk concentration in the liquid phase (C_t), and further combined with Eq. (5) to obtain ($t^* = 0$ and $q^* = 0$)

$$q_t = \frac{V_L}{m_S}\left(C_0 - \frac{(\mathbf{A}q^* + \mathbf{B})\exp[\mathbf{A}(t - t^*)]}{\mathbf{A}} + \frac{\mathbf{B}}{\mathbf{A}}\right) \tag{18}$$

$$\mathbf{A} = -\frac{k_L A}{V_L}\left(1 + \frac{V_L}{K_{11} m_S}\right) \tag{19}$$

$$\mathbf{B} = \frac{k_L A}{V_L}\left(\frac{V_L C_0}{K_{11} m_S} - \frac{K_{10}}{K_{11}}\right) \tag{20}$$

2.2 Analytical solution for continuous operation

For continuous operation, the Eqs. (1), (2), (3) and (6) can be combined in the following linear time-invariant (LTI) system

$$\frac{d\mathbf{X}}{dt} = \mathbf{A}\mathbf{X} + \mathbf{B}\mathbf{U} \tag{21}$$

$$\mathbf{A} = \begin{bmatrix} -\frac{1}{V_S}\left(\frac{k_L k_S A}{K_{11} k_S \rho + k_L} + F_S\right) & \frac{K_{11} k_S k_L A}{V_S(K_{11} k_S \rho + k_L)} \\ \frac{k_S k_L A \rho}{V_L(K_1 1 k_S \rho + k_L)} & -\frac{1}{V_L}\left(\frac{K_{11} k_S k_L A \rho}{K_{11} k_S \rho + k_L} + F_L\right) \end{bmatrix} = \begin{bmatrix} a_{11} & a_{12} \\ a_{21} & a_{22} \end{bmatrix} \tag{22}$$

$$\mathbf{B} = \begin{bmatrix} \frac{F_S}{V_S} & 0 & \frac{K_{10} k_S k_L A}{V_S(K_{11} k_S \rho + k_L)} \\ 0 & \frac{F_L}{V_L} & -\frac{K_{10} k_S k_L A \rho}{V_L(K_{11} k_S \rho + k_L)} \end{bmatrix} = \begin{bmatrix} b_{11} & b_{12} & b_{13} \\ b_{21} & b_{22} & b_{23} \end{bmatrix} \tag{23}$$

where $\mathbf{X} = [q \quad C]$ and $\mathbf{U} = [q_{in} \quad C_{in} \quad 1]$. The LTI system has the following step response solution (Ogata, 2010)

$$\mathbf{X}_t = \begin{bmatrix} q_t \\ C_t \end{bmatrix} = e^{\mathbf{A}t}\mathbf{X}_0 + \mathbf{A}^{-1}(e^{\mathbf{A}t} - \mathbf{I})\mathbf{B}\mathbf{U} \tag{24}$$

Interface variables are estimated as

$$\begin{bmatrix} q_i \\ C_i \end{bmatrix} = \mathbf{C}_1 \mathbf{X}_t + \mathbf{C}_2 \tag{25}$$

$$\mathbf{C}_1 = \begin{bmatrix} \frac{K_{11} k_S \rho}{K_{11} k_S \rho + k_L} & \frac{K_{11} k_L}{K_{11} k_S \rho + k_L} \\ \frac{k_S \rho}{K_{11} k_S \rho + k_L} & \frac{k_L}{K_{11} k_S \rho + k_L} \end{bmatrix} \tag{26}$$

$$\mathbf{C}_2 = \begin{bmatrix} \frac{K_{10} k_L}{K_{11} k_S \rho + k_L} \\ \frac{-K_{10} k_S \rho}{K_{11} k_S \rho + k_L} \end{bmatrix} \tag{27}$$

This solution, while general, cannot be used for batch operation because matrix **A** is singular when $F_L = F_S = 0$ (the equations for liquid and solid become linearly dependent). On the other hand, if the sorption isotherm is given by a piecewise linear function such as Eq. (12), the intersection is located with Eq. (13) and the time where it occurs (t_c) is now the solution of

$$\begin{bmatrix} q_{ic} \\ C_{ic} \end{bmatrix} - (\mathbf{C}_1 \mathbf{X}_t + \mathbf{C}_2) = 0 \tag{28}$$

Finally, steady-state solution can be found from Eq. (24) as ($e^{\mathbf{A}t} \to \mathbf{0}$ for an asymptotically stable LTI system)

$$\mathbf{X}_{ss} = \begin{bmatrix} q_{ss} \\ C_{ss} \end{bmatrix} = -\mathbf{A}^{-1}\mathbf{B}\mathbf{U} \tag{29}$$

2.3 Hybrid neuro-differential approach

It is possible to replace the sorption isotherm function in Eq. (4) with an ANN, resulting in a hybrid neuro-differential model. The ANN should accept C_i as the input layer and output q_i. Other inputs such as temperature could be added to the structure if necessary. The proposed regression ANN consisted of the input layer, one hidden layer, and the output layer with the following architecture ($l = 1, 2$):

$$\mathbf{a}^{[l]} = g^{[l]}(\mathbf{W}^{[l]}\mathbf{a}^{[l-1]} + \mathbf{b}^{[l]}) \tag{30}$$

where the superscript $[l]$ refers to the l-th layer of the ANN, **W** is the weight matrix, **b** is the bias vector, **a** is the activation output, and g is the activation function. In particular, $\mathbf{a}^{[0]} = f^{[0]}(C_i)$ and $\mathbf{a}^{[2]} = f^{[2]}(q_i)$ represent the normalized input and output layers, respectively, while $g^{[1]}(x) = (1 + \exp(-x))^{-1})$ is the logistic function and $g^{[2]}(x) = x$ is the identity function. Normalization between 0 and 1 is achieved by using the following relationships:

$$f^{[l]}(x) = \frac{(x - a^{[l]})}{b^{[l]}}, a^{[l]} = \min(x), b^{[l]} = \max(x) - \min(x) \tag{31}$$

where **x** is the non-normalized vector, $x = C_i$ if $f(x) = a^{[0]}$ and $x = q_i$ if $f(x) = a^{[2]}$.

3 Methods and materials

3.1 Data sources

The proposed model was used to analyze two experimental data sets from literature describing the removal of two aqueous contaminants under batch operation. The first dataset corresponds to the removal of anionic dye direct red 23 (DR23) by using graphene oxide (GO) as adsorbent (Konicki *et al.*, 2017). The second data set describes the adsorption of 4-nitrophenol (4NP) on calcium alginate-multiwall carbon nanotube beads (CAMCNB) (Ashrafi *et al.*, 2021).

3.2 Estimation of mass transfer properties from batch experiments

The analytical and hybrid neuro-differential models were iteratively solved to simultaneously estimate the mass transfer coefficients (k_S and k_L) as well as the parameters of the SLI (K_{10}, K_{11}, and K_{21}) and ANN ($\mathbf{W}^{[1]}$, $\mathbf{b}^{[1]}$, $\mathbf{W}^{[2]}$, and $b^{[2]}$) from available adsorption kinetics by minimizing the following residual sum of squares:

$$RSS = \sum_{j=1}^{M}\sum_{k=1}^{N}(q_{j,k,exp} - q_{j,k,mod})^2 \tag{32}$$

where M is the number of tested contaminant loads ($M = 5$ for the DR23 and $M = 6$ for the 4NP), N is the number of available experiment data per adsorption curve ($N = 10$ for the DR23 and $N = 9$ for the 4NP), and the subscripts *exp* and *mod* denote an experimental or a model response, respectively. Three complexity levels for the SLI were considered: (i) single segment without intercept ($q_i = K_{11}C_i$), (ii) single segment with intercept ($q_i = K_{11}C_i + K_{10}$), and a piecewise isotherm with two segments ($q_i = K_{11}C_i + K_{10}$ for $C_i > C_{ic}$ and $q_i = K_{21}C_i$ for $C_i \leq C_{ic}$). Besides, parameters were also evaluated under (i) non-negligible and (ii) negligible external resistance to mass transfer. Thus, a total of 6 scenarios were investigated during the estimation of mass transfer properties. Here, $a = 0$ and $b = 46.94$ for C_i and $a = 0$ and $b = 13.89$ for q_i for DR23, while $a = 0$ and $b = 29.20$ for C_i and $a = 0$ and $b = 136.08$ for q_i for 4NP. Both analytical and hybrid-differential models were further compared against a traditional mass transfer model formed by Eqs. (1), (2), and (3) and a non-linear equilibrium model (NLEM), given by the Langmuir isotherm:

$$q_i = \frac{q_{sat}C_i}{K_L + C_i} \tag{33}$$

Mass transfer coefficients and isotherm parameters (q_{sat}, K_L) for this scenario were estimated in the same way as the SLI and ANN cases.

The estimation of mass transfer parameters as well as the numerical solution of differential mass balances given by Eqs. (1) and (2) and the algebraic nonlinear function resulting from the combination of Eqs. (3) and (4) were implemented in the Matlab software (Matlab R2022a, MathWorks Inc., Natick, MA, USA) with routines nlinfit (Levenberg-Marquardt algorithm), ode15s (variable-order solver based on the numerical differentiation formulas), and fzero (combination of bisection, secant, and inverse quadratic interpolation methods), respectively, where the last two procedures were only required for the Langmuir and ANN isotherms. The statistical significance of estimated parameters was evaluated through their 95% confidence intervals, while the fitness quality of models was appraised with the R^2 statistics and the mean relative deviation (MRD) between experimental and fitted results.

3.3 Simulation of wastewater remediation under continuous operation

The WARM coupled to either the straight-line, ANN or Langmuir isotherms was used to simulate the evolution of the contaminant concentration in solid (q_t) and liquid (C_t) phases during the adsorption of 4NP by CAMCNB under continuous operation in three scenarios: (1) finite amount of adsorber particles in tank under fresh wastewater inflow ($F_L \neq 0$, $F_S = 0$), (2) remediation of a finite amount of wastewater under continuous replacement of adsorber in tank ($F_L = 0$, $F_S \neq 0$), and (3) fully continuous operation with both wastewater and adsorber inlet streams ($F_L \neq 0$, $F_S \neq 0$). The analytical state-space formulation given by Eqs. (24)-(27) was used to simulate the contaminant adsorption for the SLI case, while a direct numerical solution of Eqs. (1)-(4) was applied for the remaining isotherms as described for the solution of WARM under batch operation.

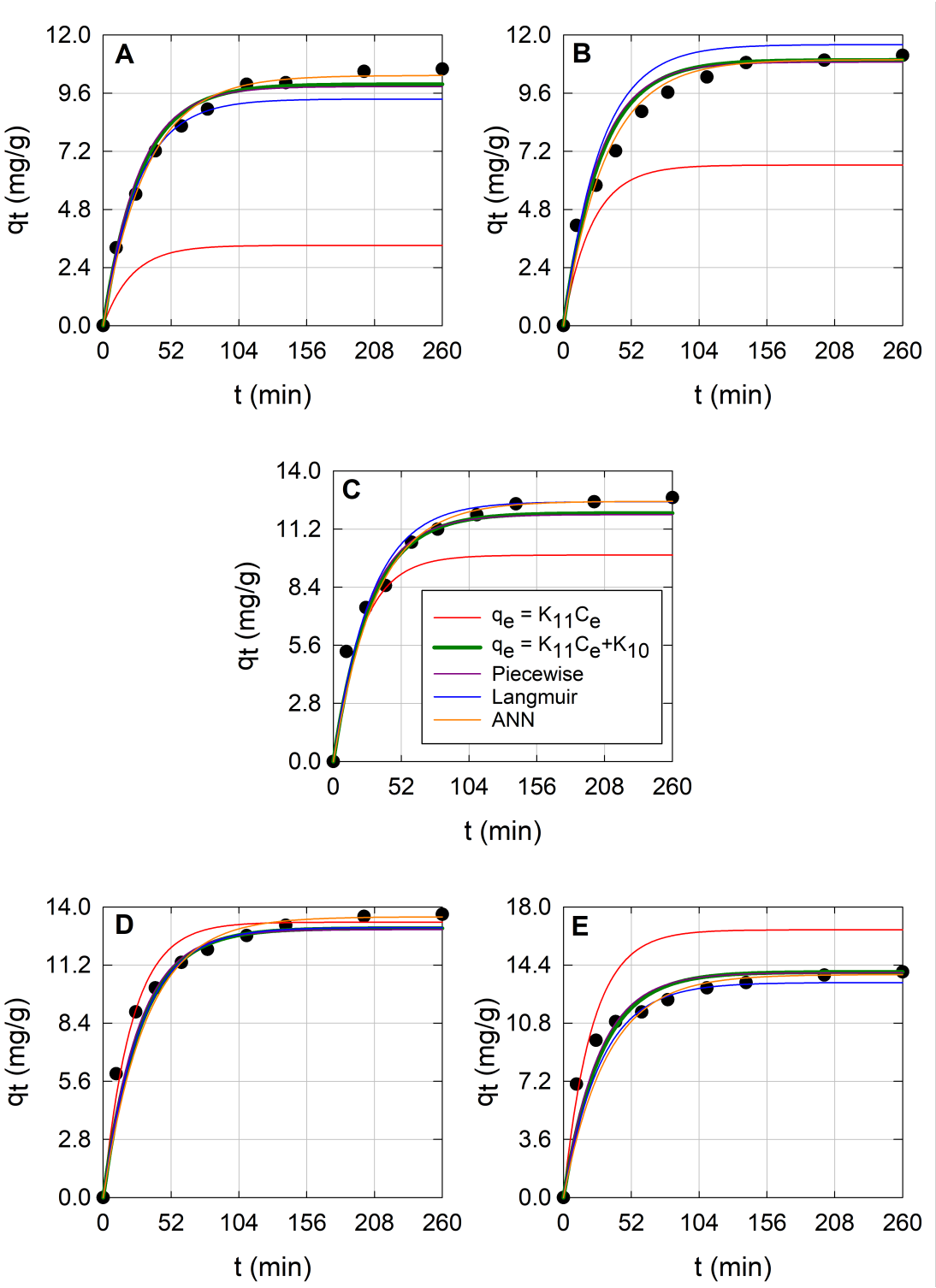

Figure 2. Experimental (dots) and fitted (lines) adsorption kinetics of anionic dye direct red 23 by graphene oxide at different starting contaminant loads. (A) 10 mg/L, (B) 20 mg/L, (C) 30 mg/L, (D) 40 mg/L, and (E) 50 mg/L. Line colors refer to the isotherm function used in the wastewater adsorption remediation model: $q_e = K_{11}C_e$ (red line), $q_e = K_{11}C_e + K_{10}$ (green line), piecewise (purple line), Langmuir (blue line), and ANN (orange line).

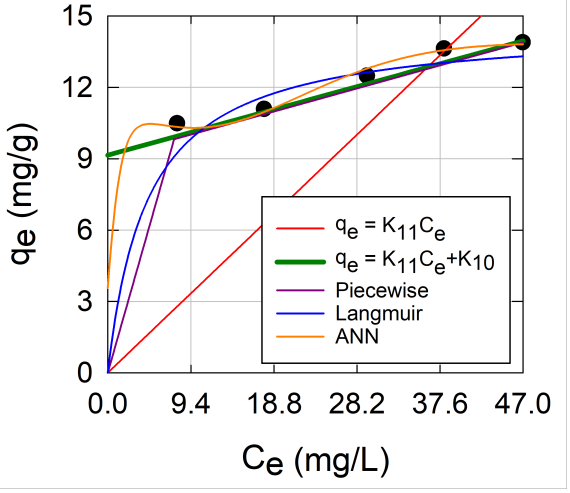

Figure 3. Experimental (dots) and fitted (lines) adsorption isotherms of anionic dye direct red 23 by graphene oxide. Isotherm functions were coupled to wastewater adsorption remediation model to allow the parameter identification only from experimental adsorption kinetics.

Finally, adsorption kinetics obtained with the straight-line and ANN isotherms were further compared to those predicted with the Langmuir equation in terms of the MRD.

4 Results and discussion

4.1 Description of batch experiments

4.1.1 DR23 removal

The experimental and fitted adsorption kinetics of DR23 by GO are shown in Figure 2, while the corresponding sorption isotherm data are shown in Figure 3. The associated experimental conditions are given in Table 1. The differential-algebraic system of equations forming the WARM was used to simultaneously identify the mass transfer coefficients (Table 2) and isotherm parameters (Table 3 and 4) only from adsorption kinetics (Figure 2). The simultaneous estimation of both internal and external mass transfer coefficients in WARM resulted in nonsignificant k_L values for all tested isotherms (Table 2, $p > 0.05$). These results validate other studies where external resistance to mass transfer is assumed when modeling adsorption kinetics (Konicki *et al.*, 2017; Ashrafi *et al.*, 2021). In this case, a special experiment design is required to isolate the contribution of adsorbent and fluid resistances to mass transfer, for example, by performing adsorption experiments at different stirring levels or by using adsorbent particles with different sizes to favor one resistance over the other. Furthermore, estimated isotherm parameters (Table 3) were unaffected by the inclusion or omission of the convective resistance to mass transfer at adsorbent surface ($p > 0.05$). The use of Langmuir and straight-line isotherms as equilibrium relationships in WARM lead to non-statistically different k_S values ($p > 0.05$), $(1.72\pm0.24)\times10^{-6}$ versus $(1.72\pm0.21)\times10^{-6}$ cm/min (one segment with intercept), respectively. On the other hand, the hybrid neuro-differential model allowed the identification of $k_L = 2.14\times10^{-3}$ cm/min and $k_S = 1.57\times10^{-6}$ cm/min ($k_L/k_S = 1363$), when both adsorbent and fluid resistances were considered in the analysis, while a $k_S = 1.50\times10^{-6}$ cm/min was obtained when external resistance was neglected. Therefore, the analytical solution to WARM coupled to a SLI represents a good alternative for the reliable estimation of mass transfer coefficients with a much

Table 1. Summary of operating conditions for investigated systems under batch operation.

Parameter	System	
	DR23/GO	4NP/CAMCNB
ρ (mg/L)	4.4E5	1.6E6
ρF_S (mg/min)	0	0
F_L (mL/min)	0	0
m_S/V_L (mg/L)	200	300
V_L (mL)	200	150
$q(t=0)$ (mg/g)	0	0
$C(t=0)$ (mg/L)	10, 20, 30, 40, and 50	5, 10, 15, 25, 50, and 70
q_{in} (mg/g)	0	0
C_{in} (mg/L)	0	0

Table 2. Mass transfer coefficients identified during adsorption of anionic direct red 23 by graphene oxide and 4-nitrophenol on calcium alginate-multiwall carbon nanotube beads.

System	Parameter	$q_e = K_{11}C_e$	$q_e = K_{11}C_e + K_{10}$	Piecewise	ANN	Langmuir
DR23/GO	Simultaneous external (convective) and internal resistances are considered					
	$k_L \times 10^3$ (cm/min)	**7.2** $\times 10^{5a}$	**4.9** $\times 10^{6a}$	**1.1** $\times 10^{6a}$	**2.14**^{a}	**-392.9**^{a}
	$k_S \times 10^6$ (cm/min)	2.09 ± 1.18	1.73 ± 0.22	1.80 ± 0.29	1.57 ± 0.35	1.74 ± 0.26
	Internal resistance is considered while convective resistance is neglected					
	$k_S \times 10^6$ (cm/min)	2.14 ± 1.19	1.72 ± 0.21	1.83 ± 0.25	1.50 ± 0.18	1.72 ± 0.24
4NP/ CAMCNB	Simultaneous external (convective) and internal resistances are considered					
	$k_L \times 10^1$ (cm/min)	**3.64**^{a}	**4.00**^{a}	**22.6**^{a}	3.32 ± 1.04	2.40 ± 0.29
	$k_S \times 10^5$ (cm/min)	**4.22**^{a}	4.61 ± 4.19	4.11 ± 0.74	5.18 ± 0.84	4.92 ± 0.73
	Internal resistance is considered while convective resistance is neglected					
	$k_S \times 10^5$ (cm/min)	1.28 ± 0.72	2.50 ± 0.68	3.94 ± 0.66	3.67 ± 0.46	3.84 ± 0.54

[a]Bold number indicates nonsignificant parameter estimates ($p > 0.05$).

Table 3. Isotherm parameters describing the equilibrium adsorption of anionic direct red 23 by graphene oxide and 4-nitrophenol on calcium alginate-multiwall carbon nanotube beads.

System	Isotherm parameter	$q_e = K_{11}C_e$	$q_e = K_{11}C_e + K_{10}$	Piecewise Langmuir	
DR23/GO	Simultaneous external (convective) and internal resistances are considered				
	$K_{11} \times 10^{-2}$ (cm^3/g)	3.60 ± 0.54	1.03 ± 0.21	1.02 ± 0.21	-
	$K_{10} \times 10^3$ (g/g)	-	9.16 ± 0.73	9.11 ± 0.95	-
	$K_{21} \times 10^{-3}$ (cm^3/g)	-	-	**1.29**^{a}	-
	$q_{sat} \times 10^2$ (g/g)	-	-	-	1.46 ± 0.10
	$K_L \times 10^6$ (cm^3/g)	-	-	-	4.59 ± 1.75
	Internal resistance is considered while convective resistance is neglected				
	$K_{11} \times 10^{-2}$ (cm^3/g)	3.55 ± 0.46	1.02 ± 0.21	1.03 ± 0.20	-
	$K_{10} \times 10^3$ (g/g)	-	9.15 ± 0.66	9.05 ± 0.91	-
	$K_{21} \times 10^{-3}$ (cm^3/g)	-	-	**1.31**^{a}	-
	$q_{sat} \times 10^2$ (g/g)	-	-	-	1.46 ± 0.09
	$K_L \times 10^6$ (cm^3/g)	-	-	-	4.54 ± 1.56
4NP/CAMCNB	Simultaneous external (convective) and internal resistances are considered				
	$K_{11} \times 10^{-3}$ (cm^3/g)	6.82 ± 2.17	4.37 ± 0.98	0.98 ± 0.50	-
	$K_{10} \times 10^1$ (g/g)	-	0.36 ± 0.11	1.11 ± 0.12	-
	$K_{21} \times 10^{-4}$ (cm^3/g)	-	-	2.30 ± 1.01	-
	$q_{sat} \times 10^1$ (g/g)	-	-	-	1.52 ± 0.12
	$K_L \times 10^6$ (g/cm^3)	-	-	-	3.41 ± 0.25
	Internal resistance is considered while convective resistance is neglected				
	$K_{11} \times 10^{-3}$ (cm^3/g)	11.7 ± 4.08	4.35 ± 0.77	0.99 ± 0.50	-
	$K_{10} \times 10^1$ (g/g)	-	0.36 ± 0.10	1.11 ± 0.12	-
	$K_{21} \times 10^{-4}$ (cm^3/g)	-	-	2.18 ± 0.85	-
	$q_{sat} \times 10^1$ (g/g)	-	-	-	1.63 ± 0.10
	$K_L \times 10^6$ (g/cm^3)	-	-	-	4.21 ± 1.40

[a]Bold number indicates nonsignificant parameter estimates ($p > 0.05$).

simpler approach that can be implemented even in a spreadsheet with an optimization tool such as the Excel Solver.

Since convective resistance to mass transfer was proven negligible under the explored conditions, the remaining discussion is focused to results obtained by assuming an instantaneous mass equilibrium of adsorbent surface. Isotherm parameters are summarized in Table 3 for all but the ANN isotherm, whose results are in turn presented in Table 4. The ability of WARM to accurately describe adsorption kinetics (Figure 2) can be explained in terms of how well the chosen isotherm equation, identified from dynamic experiments, describes the equilibrium values (Figure 3). Thus, fitness quality indices (R^2 and MRD) for isotherm curves were quantified in addition to those for adsorption kinetics. The proposed analytical solution reproduced the experimental dynamic and equilibrium behavior with different fitness quality levels depending on the structure of

Table 4. ANN parameters describing the equilibrium adsorption of anionic direct red 23 by graphene oxide and 4-nitrophenol on calcium alginate-multiwall carbon nanotube beads.

System	Simultaneous external (convective) and internal resistances are considered	Internal resistance is considered while convective resistance is neglected
DR23/GO	$\mathbf{W}^{[1]T}$= [0.10, 1.26, 26.44, 21.02, 4.61, 6.11]; $\mathbf{b}^{[1]T}$= [0.29, 0.62, 0.41, -0.45, -1.64, -0.82]; $\mathbf{W}^{[2]}$ = [-1.44, -0.43, 1.81, 0.06, 0.83, -0.44]; $\mathbf{b}^{[2]}$ = [0]	$\mathbf{W}^{[1]T}$= [0.11, 0.99, 45.40, -1.02, 5.09, 8.19]; $\mathbf{b}^{[1]T}$= [0.34, 0.66, 0.92, -0.14, -1.87, -0.75]; $\mathbf{W}^{[2]}$ = [-1.25, -0.54, 1.91, 0.01, 0.70, -0.37]; $\mathbf{b}^{[2]}$ = [0]
4NP/ CAMCNB	$\mathbf{W}^{[1]T}$= [-10.74, -1.95, 151.04, -1.78, -0.36, 0.90, -11.35]; $\mathbf{b}^{[1]T}$= [-2.11, 6.59, 1.69, -0.15, -1.37, 0.53, 0.63]; $\mathbf{W}^{[2]}$ = [-0.23, 0.57, 0.62, -0.60, -0.23, -0.10, -0.89]; $\mathbf{b}^{[2]}$ = [0]	$\mathbf{W}^{[1]T}$= [-10.05, -2.25, 126.12, -2.06, -0.37, 1.20, -12.06]; $\mathbf{b}^{[1]T}$= [-2.69, 10.04, 1.38, -0.20, -1.29, 0.94, 0.60]; $\mathbf{W}^{[2]}$ = [-0.12, 0.60, 0.65, -0.76, -0.21, -0.10, -0.97]; $\mathbf{b}^{[2]}$ = [0]

the chosen isotherm (Table 5). For the adsorption kinetics, the lowest fitness quality was exhibited by wastewater model coupled to the SLI without intercept ($q_e = K_{11}C_e$, K_{11} = 3.55×10^2 cm^3/g) with MRD values about 29% (R^2= 0.36, red line in Figure 2). The addition of an intercept to the SLI ($q_e = K_{11}C_e + K_{10}, K_{11}$ = 1.02×10^2 cm^3/g and K_{10}= 9.15×10^{-3} g/g) increased its prediction capabilities reducing observed deviations to about 7.3% (R^2 = 0.96, green line in Figure 2). Switching to a piecewise SLI such as that given by Eq. (12), with K_{20} = 0 (K_{11} = 1.03×10^2 cm^3/g, K_{10} = 9.05×10^{-3} g/g, and K_{21} = 1.31×10^3 g/g), did not significantly improve the description of dynamic data (MRD and R^2 values remained practically unchanged). The poor description capabilities of adsorption kinetics by wastewater model coupled to zero-intercept SLI, are explained by the failure of this isotherm to describe equilibrium data (MRD= 30.9%, red line in Figure 3). On the other hand, the SLI with intercept was able to closely follow all the available equilibrium data for DR23 removal (MRD= 2.77%, R^2>0.91, green line in Figure 3), contributing to the observed improvement over the SLI with zero intercept, even if it does not asymptotically approach the origin as expected from an isotherm model. Finally, the piecewise SLI overlapped to the single straight-line one for much of the concentration range (green line in Figure 3) and statistical analysis identified a nonsignificant estimation of the second segment (Table 3, $p > 0.05$), that is, the second section of the SLI was not necessary for a good reproduction of the experimental behavior.

Regarding the hybrid neuro-differential approach, the use of an ANN isotherm (Table 4) reduced average deviations to about 7% (R^2 = 0.96, orange lines in Figure 2) when describing the adsorption kinetics,

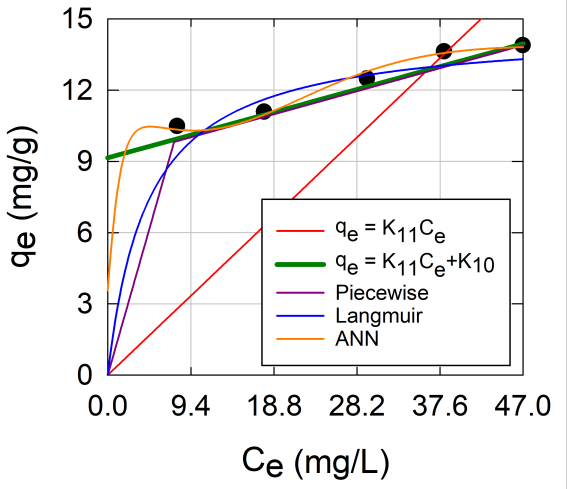

Figure 3. Experimental (dots) and fitted (lines) adsorption isotherms of anionic dye direct red 23 by graphene oxide. Isotherm functions were coupled to wastewater adsorption remediation model to allow the parameter identification only from experimental adsorption kinetics.

while deviations near to 1% (R^2 = 0.98) were achieved for the description of the equilibrium behavior (orange line in Figure 3). Finally, the Langmuir isotherm (q_{sat} = 1.46×10^{-2} g/g and K_L = 4.54×10^{-6} cm^3/g) contributed to a good reproduction of the dynamic period by WARM (blue line in Figure 2) with a MRD close to 8% (R^2 = 0.95). Nevertheless, while the equilibrium period was described with an error close to 5% (blue line in Figure 3), the proportion of explained variance achieved by this model as quantified by the R^2 index was about the 70%. It is evident that equilibrium adsorption of dye DR23 by GO does not

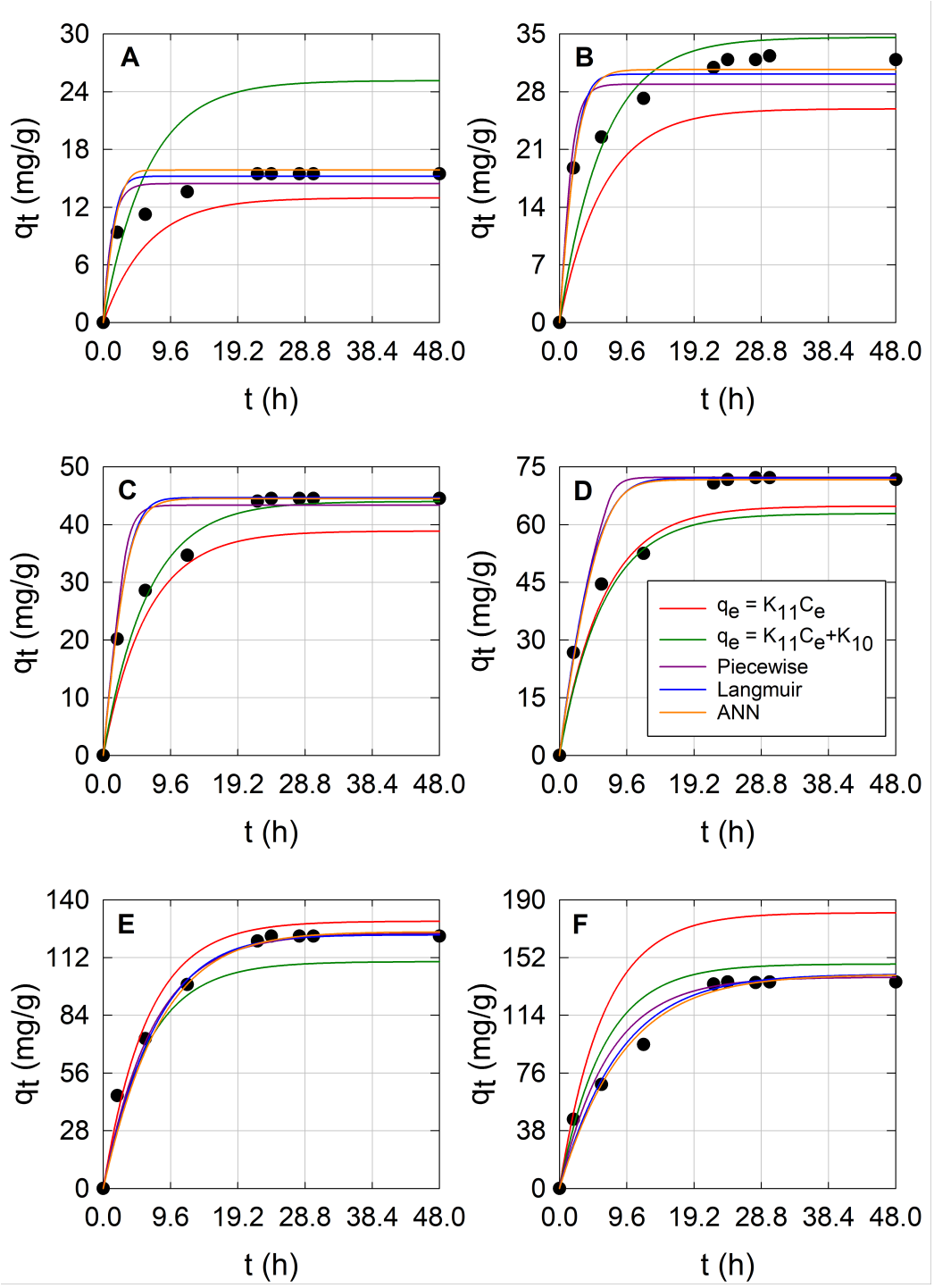

Figure 4. Experimental (dots) and fitted (lines) adsorption kinetics of 4-nitrophenol on calcium alginate-multiwall carbon nanotube beads at different starting contaminant loads. (A) 5 mg/L, (B) 10 mg/L, (C) 15 mg/L, (D) 25 mg/L, (E) 50 mg/L, and (F) 70 mg/L. Line colors refer to the isotherm function used in the wastewater adsorption remediation model: $q_e = K_{11}C_e$ (red line), $q_e = K_{11}C_e + K_{10}$ (green line), piecewise (purple line), Langmuir (blue line), and ANN (orange line).

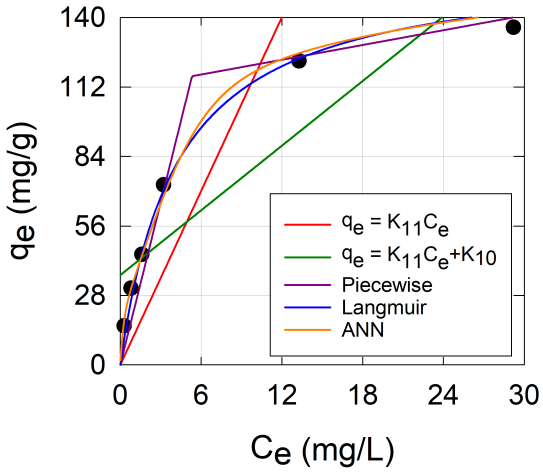

Figure 5. Experimental (dots) and fitted (lines) adsorption isotherms of 4-nitrophenol on calcium alginate-multiwall carbon nanotube beads. Isotherm functions were coupled to wastewater adsorption remediation model to allow the parameter identification only from experimental adsorption kinetics.

seem to reach an asymptotic (saturation) region such as that predicted by the Langmuir isotherm (Figure 3), thus explaining its inferior capacity to describe this system.

4.1.2 4NP removal

Experimental and fitted adsorption curves for dynamic and equilibrium adsorption of 4NP by CAMCNB are shown in Figures 4 and 5, respectively. Experimental conditions for this case are listed in Table 1. Like the DR23 case, the identified k_L/k_S ratio was very large (>1000) for all tested isotherms (Table 2), indicating a negligible resistance to mass transfer in the fluid phase. Thus, the omission of convective resistance is also justified in this scenario and discussion will be centered in these results. The use of the piecewise, ANN, and Langmuir isotherms in WARM allowed the identification of very close k_S values, $(3.94\pm0.66)\times10^{-5}$ versus $(3.67\pm0.46)\times10^{-5}$ versus $(3.84\pm0.54)\times10^{-5}$ cm/min, respectively. In contrast, lower k_S values were estimated when differential-algebraic system was coupled to the single segment SLI equations, albeit in the same magnitude order. The SLI without intercept lead to a k_S value of $(1.28\pm0.72)\times10^{-5}$ cm/min, while its non-zero intercept counterpart produced a value of $(2.50\pm0.68)\times10^{-5}$ cm/min. However, these last values could be discarded because the inferior ability of WARM and SLI equations to describe the adsorption kinetics and adsorption isotherm behavior, respectively (Table 5). The worst description of the dynamic elimination of 4NP with CAMCNB was exhibited by WARM coupled to the SLI without intercept ($q_e = K_{11}C_e, K_{11} = 11.7\times10^3$ cm^3/g), with a MRD of 21% ($R^2 = 0.84$, red line in Figure 4).

Table 5. Fitness quality indices achieved by the wastewater remediation model for the description of dynamic and equilibrium adsorption of anionic direct red 23 by graphene oxide and 4-nitrophenol on calcium alginate-multiwall carbon nanotube beads[a].

System	Coupled isotherm	Simultaneous external (convective) and internal resistances are considered		Internal resistance is considered while convective resistance is neglected	
		Adsorption kinetics	Equilibrium curve	Adsorption kinetics	Equilibrium curve
DR23/GO	$q_e = K_{11}C_e$	28.9/0.36	30.7/ – 9.32	28.9/0.36	30.9/ – 9.39
	$q_e = K_{11}C_e + K_{10}$	7.32/0.96	2.69/0.92	7.34/0.96	2.77/0.91
	Piecewise	7.29/0.96	3.01/0.90	7.27/0.96	3.25/0.88
	ANN	6.98/0.96	1.43/0.98	6.98/0.95	1.21/0.98
	Langmuir	8.37/0.95	5.31/0.71	8.35/0.95	5.26/0.72
4NP/CAMCNB	$q_e = K_{11}C_e$	25.8/0.92	64.5/0.22	21.0/0.84	71.9/-2.72
	$q_e = K_{11}C_e + K_{10}$	19.0/0.95	40.4/0.79	19.2/0.96	40.8/0.79
	Piecewise	8.96/0.98	20.2/0.97	9.96/0.98	22.0/0.97
	ANN	7.71/0.99	10.77/0.98	8.86/0.98	4.63/0.99
	Langmuir	16.6/0.88	7.24/1.00	8.89/0.98	9.74/0.99

[a]Values expressed as MRD (%)/R^2.

Unlike the analysis of DR23 adsorption unto GO, the addition of an intercept to the SLI ($q_e = K_{11}C_e + K_{10}, K_{11}$= 4.35×10^3 cm^3/g and K_{10} = 0.36×10^1 g/g) did not significantly improve the description of dynamic mass transfer. In this case, observed deviations only reduced to about 19% (R^2 = 0.96, green lines in Figure 4), and the use of a piecewise SLI (K_{11} = 0.99×10^3 cm^3/g, K_{10} = 1.11×10^{-1} g/g, K_{21} = 2.18×10^4 g/g, and K_{20} = 0) was necessary to reduce MRD values to about 10% (R^2 = 0.98, purple lines in Figure 4). The mathematical description of mass transfer equilibrium is useful to understand these results. SLI without intercept achieved a poor description of equilibrium data, with errors in the order of 72% (red line in Figure 5). The SLI with non-zero intercept improved the equilibrium description, but average differences between experimental and predicted results were still near 40% (R^2 = 0.79, green line in Figure 5), also affecting the description of dynamic behavior. Thus, the addition of a second segment to SLI was paramount to closely follow the experimental equilibrium behavior (about 20% deviation, R^2 = 0.97, purple line in Figure 5) and improve the description of adsorption kinetics. A comparable description of dynamic data was achieved by wastewater model coupled to the Langmuir isotherm (q_{sat} = 1.63×10^{-1} g/g and K_L = 4.21×10^{-6} cm^3/g, blue line in Figure 4), but deviation was lower when considering the equilibrium data (about 10%, blue line in Figure 5). The mass transfer model coupled with the Langmuir isotherm was bested by the hybrid neuro-differential model, albeit by a very small margin, with an average deviation close to 9% for adsorption kinetics (R^2 = 0.98, orange lines in Figure 4) and about 5% for equilibrium curves (R^2 = 0.99, orange line in Figure 5).

ANN have been successfully used to describe both equilibrium and dynamic data for wastewater remediation. Several approaches can be followed for the description of sorption isotherms for single and multiple component systems, for example, q_e and C_e can be directly related by the ANN (Mendoza-Castillo *et al*., 2018), that is, the approach followed in this study where the ANN is the isotherm. However, ANN can be also used to vary the parameters of a traditional isotherm model such as the Langmuir or Sips isotherms and introduce the effect of additional factors (Fagundez *et al*., 2021). The input-output relationship in ANN is highly nonlinear due to the complex neuron interactions in layers as well as the saturating nature of some activation functions. This nonlinearity can lead to physically inconsistent behaviors when modeling complex systems such as multicomponent adsorption (Mendoza-Castillo *et al*., 2018). However, resulting neural isotherms are never tested in dynamic simulations, a trend also extended to traditional isotherms, where the nonlinearity of the equilibrium model is added to the iterative solution of differential and algebraic mass balances, increasing the possibility of multiple state trajectories. On the other hand, the modeling of the dynamic adsorption by ANN is performed by ignoring the equilibrium relationship between the solid and liquid phases; here the contact time is used as an input variable for batch (Marzban *et al*., 2021) and continuous (Chowdhury and Saha, 2013) adsorption systems, but only under the continuous feed of wastewater in the second case. The problem with these models is that they are not generalizable to other process conditions: ANN for batch processes lack input variables for continuous operation, or the ANN for a packed column cannot be used to explore scenarios where the system also possesses an adsorber inflow. Besides, these ANN does not incorporate design variables beyond those explored in the experiments. Therefore, analyzing a hybrid-differential approach where the ANN isotherm is incorporated in a model resulting from mass balances in the adsorption system, such as that proposed in current study, is desirable because it provides generality to describe a wider range of operation conditions.

4.2 Simulation of continuous operation

The simulated evolution of the contaminant concentration in solid (q_t) and liquid (C_t) phases during the 4NP adsorption on CAMCNB under continuous operation are shown in Figure 6 for the three tested scenarios. All simulations were obtained with a unique k_S value (3.94×10^{-5} cm/min) as no significant differences were found in estimates of this parameter when the WARM was coupled to piecewise, ANN, or Langmuir isotherms during the analysis of batch experiments. Besides, a large k_L-to-k_S ratio (10000) was considered since external resistance to mass transfer was also proven negligible. The remaining parameters used in these simulations are listed in Table 6. The simulations of contaminant concentration where a fresh wastewater stream enters a tank containing a finite amount of adsorber particles ($F_L \neq 0$, $F_S = 0$) is presented in Figures 6A and 6B for the solid (q_t) and liquid (C_t) phases, respectively.

Table 6. Summary of parameters for the simulation of 4-nitrophenol adsorption on calcium alginate-multiwall carbon nanotube beads under continuous operation.

System description	Case 1. Finite amount of adsorber particles in tank under fresh wastewater inflow ($F_L \neq 0$, $F_S = 0$)	Case 2. Remediation of a finite amount of wastewater under continuous replacement of adsorber in tank ($F_L = 0$, $F_S \neq 0$)	Case 3. Fully continuous operation with both wastewater and adsorber inlet streams ($F_L \neq 0$, $F_S \neq 0$)
ρF_S (mg/min)	0	0.8	0.8
F_L (mL/min)	3	0	3
Shared properties and operating conditions	ρ (mg/L) = 1.6E6, m_S/V_L (mg/L) = 300, V_L (mL) = 150, $q(t=0)$ (mg/g) = 0, $C(t=0)$ (mg/L) = 30, q_{in} (mg/g) = 0, C_{in} (mg/L) = 30, k_S (cm/min) = $3.94\times10{-}5a$, k_L (cm/min) = $10000k_S$		
Piecewise isotherm[b]	$K_{11} = 0.99\times10^{3}$ cm^3/g, $K_{10} = 1.11\times10^{-1}$ g/g, $K_{21} = 2.18\times10^{4}$ g/g, and $K_{20} = 0$		
ANN isotherm[b]	$\mathbf{W}^{[1]T}$= [-10.05, -2.25, 126.12, -2.06, -0.37, 1.20, -12.06]; $\mathbf{b}^{[1]T}$= [-2.69, 10.04, 1.38, -0.20, -1.29, 0.94, 0.60]; $\mathbf{W}^{[2]}$ = [-0.12, 0.60, 0.65, -0.76, -0.21, -0.10, -0.97]; $\mathbf{b}^{[2]}$ = [0]		
Langmuir isotherm[b]	$q_{sat} = 1.63\times10^{-1}$ g/g and $K_L = 4.21\times10^{-6}$ cm^3/g		

[a]Estimated during the analysis of batch experiments with wastewater remediation model coupled to piecewise isotherm. [b]Identified with the wastewater remediation model by neglecting convective resistance to mass transfer during the analysis of batch experiments.

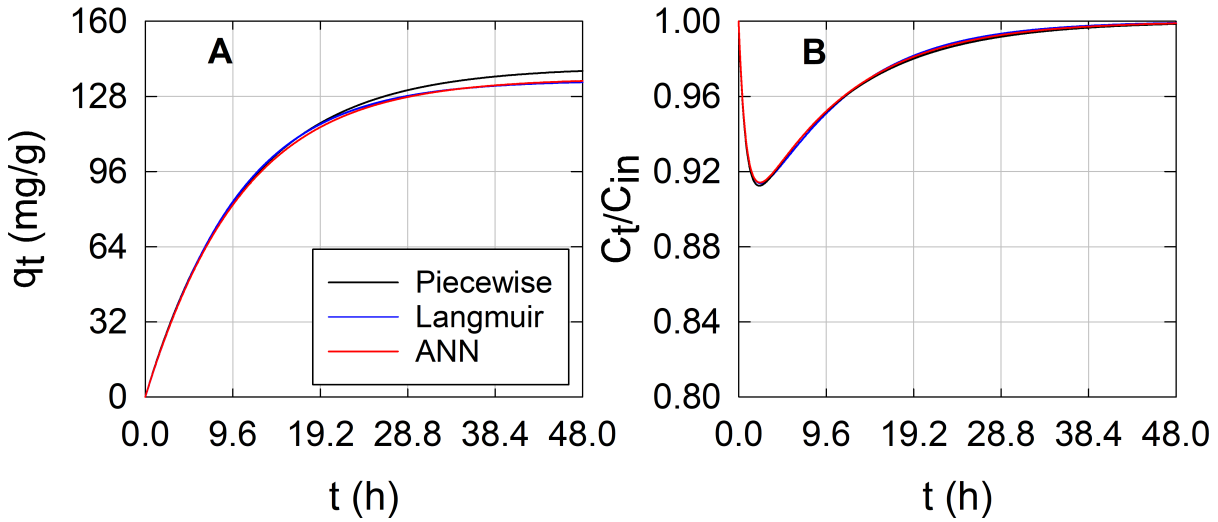

Figure 6. Predicted adsorption kinetics of 4-nitrophenol on calcium alginate-multiwall carbon nanotube beads under a finite amount of adsorber particles in tank with fresh wastewater inflow. Pollutant concentration in (A) adsorber particles in tank and (B) liquid outflow. Line colors refer to the isotherm function used in the wastewater adsorption remediation model: piecewise (black line), Langmuir (blue line), and ANN (red line).

The plot of q_t versus t for WARM coupled to SLI (black line) differs in 1.57% to that obtained when the Langmuir isotherm is used (blue line), while a 0.74% difference exists between simulations incorporating the ANN (red line) and Langmuir isotherms. Removal of contaminants from wastewater under continuous liquid inflow has been investigated in both packed columns (fixed bed) (Biswas and Mishra, 2015) and completely mixed reactors (Obón *et al.*, 2022). These systems are very often characterized in terms of the breakthrough curve, an experiment where tank is initially filled with pure water ($C(t = 0) = 0$) and the inlet stream is subjected to a step disturbance by switching from a clean inflow to other containing the pollutant (Chowdhury *et al.*, 2013). The qualitative behavior of the outlet wastewater concentration for this case (Figure 6B) resembles that obtained in those studies, with the major difference being the starting state for liquid phase: the adsorber tank was initially filled with wastewater in this work

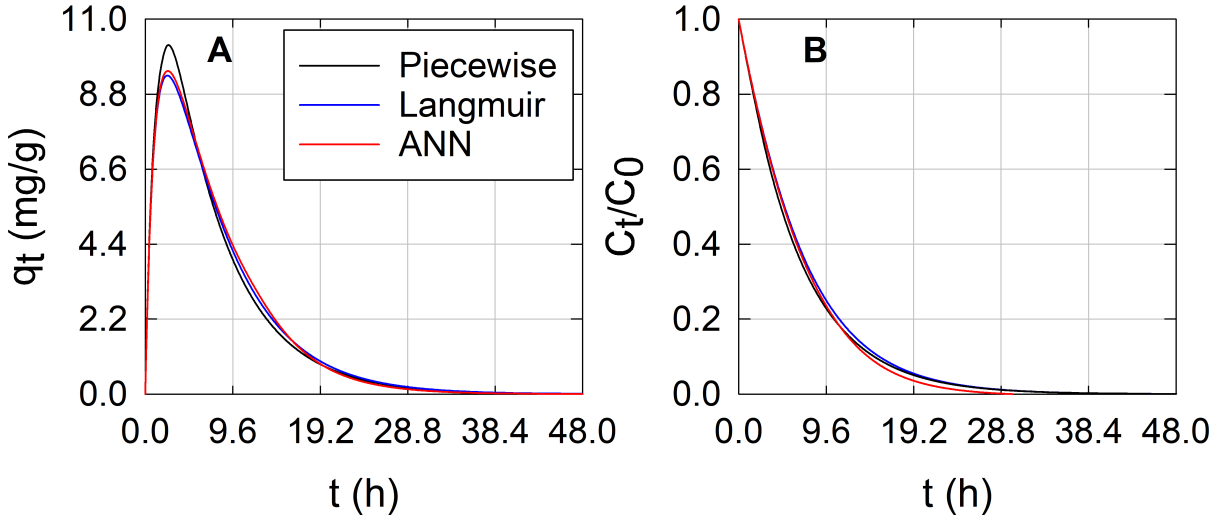

Figure 7. Predicted adsorption kinetics of 4-nitrophenol on calcium alginate-multiwall carbon nanotube beads during remediation of a finite amount of wastewater under continuous replacement of adsorber in tank. Pollutant concentration in (A) adsorber particles at outlet stream and (B) liquid in tank. Line colors refer to the isotherm function used in the wastewater adsorption remediation model: piecewise (black line), Langmuir (blue line), and ANN (red line).

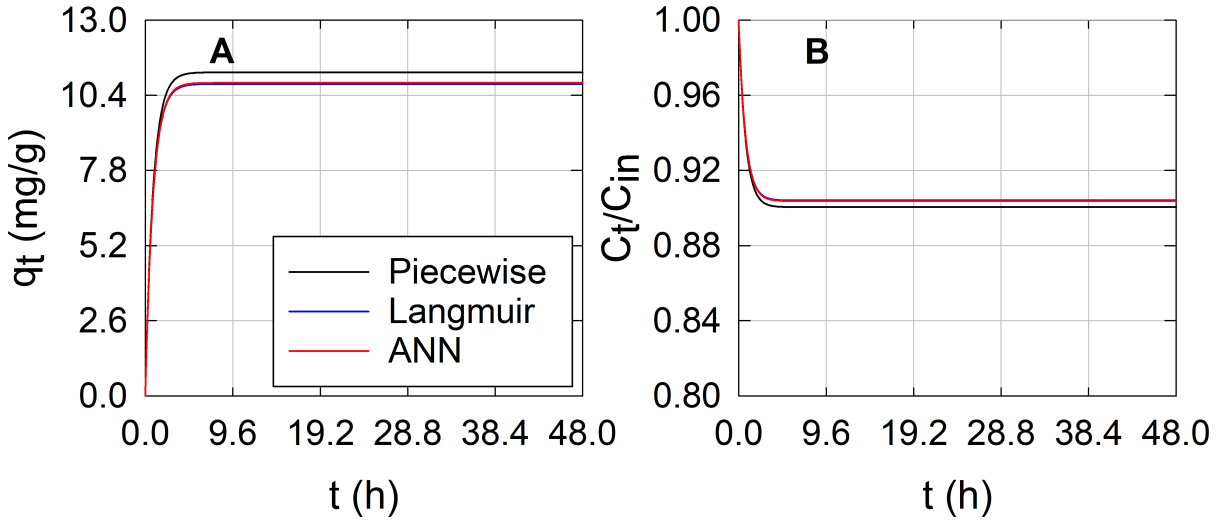

Figure 8. Predicted adsorption kinetics of 4-nitrophenol on calcium alginate-multiwall carbon nanotube beads under continuous operation with simultaneous wastewater and adsorber inlet streams. Pollutant concentration in (A) adsorber particles and (B) liquid at outlet streams. Line colors refer to the isotherm function used in the wastewater adsorption remediation model: piecewise (black line), Langmuir (blue line), and ANN (red line).

($C(t = 0) \neq 0$). The adsorbent gradually saturates because it is never replaced (Figure 6A), while the liquid phase evolves toward the conditions of the inlet stream (Verduzco-Navarro *et al.*, 2020a). The outlet concentration immediately increases if the system is fully mixed, as observed by Obón *et al.* (2022) while prototyping a spinning adsorber submerged filter for the continuous removal of azorubine with

granulated activated carbon. However, a lag phase manifests in the outlet concentration when the fully mixed assumption is not satisfied, for example, in packed beds, where plug flow is very likely to occur for increasing diameter-to-length ratios (Verduzco-Navarro *et al*., 2020b, Fadzail *et al*., 2022). The proposed model was developed under a fully mixed assumption, but it can be easily adapted to consider deviations from this state or to approach plug-flow by modeling the adsorber as a series of ideally mixed stages also having a state-space solution due to its linear nature.

The second scenario considers the remediation of a finite amount of wastewater contained in a tank with continuous feed of the adsorbent material ($F_L = 0$, $F_S \neq 0$). As opposed to the previous case, the adsorbent at the outlet gradually increases its contaminant load but eventually leaves the system without pollutant traces as it is constantly replaced from the system (Figure 7A), allowing to fully eliminate the pollutant from the liquid phase (Figure 7B). In this case, the ANN produced negative steady-state values for C_t (≈ -0.15), instead of asymptotically approach a zero value. This result occurs because ANN does not fully converge to the origin in Figure 5, but to $q_e = 1.83$ mg/g when $C_e = 0$ mg/L, a physical inconsistency inexistent with straight-line and Langmuir isotherms.

The last scenario considers that adsorbent and wastewater streams enter simultaneously the remediation tank. Steady-state outlet conditions are reached in solid (Figure 8A) and liquid (Figure 8B) phases. This scenario and the previous one are interesting from a scale up perspective because they reduce the time needed for replacing adsorbent in tank; nevertheless, to the best of the authors' knowledge these cases have yet to be investigated in literature. In all cases, the proposed analytical state-space solution exhibited a behavior comparable to that numerically obtained by using the other NLEM. Adsorption kinetics in solid phase (Figures 6A, 7A and 8A) obtained by using the piecewise isotherm in WARM (black line) differed in 1.57, 6.31, and 5.04% to those obtained by applying the Langmuir isotherm (black line) for cases 1 ($F_L \neq 0$, $F_S = 0$), 2 ($F_L = 0$, $F_S \neq 0$), and 3 ($F_L \neq 0$, $F_S \neq 0$), respectively, while MRD values between WARM incorporating the ANN and Langmuir isotherms were 0.74 (case 1), 2.18 (case 2), and 1.65% (case 3). On the other hand, differences between the solution obtained by coupling the Langmuir isotherm to WARM and those corresponding to the piecewise or ANN isotherms in the liquid phase (Figures 6B, 7B and 8B) were 0.06, 4.06, and 0.52% and 0.04, 4.08, 0.17% for the cases 1, 2, and 3, respectively.

Results in this section demonstrate that the use of a SLI in WARM allows to obtain results comparable to the use of other NLEM, but with a much lower computational effort, as the analytical solution eliminates the need of solving a differential model coupled to a nonlinear algebraic equation. Besides, the hybrid neuro-differential approach allows the use of an ANN isotherm to describe batch and continuous operation modes. In addition, state-space formulations such as that given in Eqs. (21) to (23) can be applied to design popular linear controllers, such as PI or PID ones, by using well-known state-space methods for LTI representations and further examine their stability, performance, and robustness (Hernández-Osorio *et al*., 2020).

Conclusions

The mass transfer model coupled to the SLI can describe both the dynamic and equilibrium adsorption of contaminants from wastewater under continuous and batch operations. The precision of this model is comparable to that obtained by using other NLEM such as the Langmuir and ANN isotherms. However, due to its analytical nature, the proposed solution eliminates the need for the numerical solution of differential mass balances and algebraic nonlinear function at solid-liquid interface. For continuous operation, the analytical model offers an additional advantage over their nonlinear counterparts as it can be easily applied in the synthesis of automatic control systems. Finally, results demonstrated that the hybrid neuro-differential model resulting from combining an ANN isotherm and mass balances in the adsorption system can be generalized to batch and continuous operations. Thus, this approach can be followed to describe complex equilibrium interactions such as those arising in multicomponent systems.

Acknowledgments

Daniel Temoltzin Lobatón acknowledges his post-graduate scholarship from CONACYT (Grant number 1070865). Dr. Irving Israel Ruiz-López thanks the VIEP-BUAP for providing financial support trough project 100474666-VIEP2022, respectively.

Nomenclature

a, b	coefficients of the normalization function
a	activation output
A	adsorbent area (m^2)
A	state coefficients matrix
b	bias vector
B	input coefficients matrix
C	contaminant concentration in liquid phase (mg/L)
$\mathbf{C}_1$,$\mathbf{C}_2$	interface coefficients matrices
$f^{[]}$	normalization function in the ANN
F	flow rate (L/s)
g	activation function
I	identity matrix
k	mass transfer coefficient (m/s)
K_L	parameter for Langmuir isortherm (mg/L)
K_{j1}	denotes the slope of the j-th segment in straight-line isotherm
K_{j0}	denotes the intercept of the j-th segment in straight-line isotherm
m	mass (g)
M	number of tested contaminant loads
N	number of available experiment data per adsorption curve
q	contaminant concentration in solid phase (mg/g)
q_{sat}	maximum adsorption capacity in Langmuir isotherm (mg/g)
t	time (s)
U	input vector
V	volume (L)
W	weight matrix
x	non-normalized vector
Greek symbols	
ρ	density (kg/m^3)
Subscripts	
0	denotes an initial state
c	denotes the intersection of straight-line isotherms
e	denotes the equilibrium
exp	denotes an experimental value
i	denotes the solid-liquid interface
in	denotes the inlet stream
L	denotes the liquid phase
mod	denotes a model value
S	denotes the solid phase
ss	denotes the steady-state
t	at time t
Superscripts	
$[l]$	denotes the l-th layer of the ANN
*	denotes a lower integral limit

References

Aggelopoulos, C.A. (2022). Recent advances of cold plasma technology for water and soil remediation: A critical review. *Chemical Engineering Journal 428*, 131657. https://doi.org/10.1016/j.cej.2021.131657

Ahmed, M., Mavukkandy, M.O., Giwa, A., Elektorowicz, M., Katsou, E., Khelifi, O., Naddeo, V. and Hasan, S.W. (2022). Recent developments in hazardous pollutants removal from wastewater and water reuse within a circular economy. *NPJ Clean Water 5*, 12. https://doi.org/10.1038/s41545-022-00154-5

Ashrafi, S.D., Safari, G.H., Sharafi, K., Kamani, H. and Jaafari, J. (2021). Adsorption of 4-Nitrophenol on calcium alginate-multiwall carbon nanotube beads: Modeling, kinetics, equilibriums and reusability studies. *International Journal of Biological Macromolecules 185*, 66-76. https://doi.org/10.1016/j.ijbiomac.2021.06.081

Ayouch, I., Barrak, I., Kassab, Z., El Achaby, M., Barhoun, A. and Draoui, K. (2020). Impact of the drying process on the efficiency of alginate beads for cadmium removal from water: Kinetic, isotherm and thermodynamic study. *Environmental Technology and Innovation 20*, 101157. https://doi.org/10.1016/j.eti.2020.101157

Biswas, S. and Mishra, U. (2015). Continuous fixed-bed column study and adsorption modeling: removal of lead ion from aqueous solution by charcoal originated from chemical carbonization of rubber wood sawdust. *Journal of Chemistry*, Article ID 907379. http://dx.doi.org/10.1155/2015/907379

Castillo-Santos, K., Ruiz-López, I.I., Rodríguez-Jiménez, G.C., Carrillo-Ahumada, J. and García-Alvarado, M.A. (2017). Analysis of mass transfer equations during solid-liquid extraction and its application for vanilla extraction kinetics modeling. *Journal of Food Engineering 192*, 36-44. http://dx.doi.org/10.1016/j.jfoodeng.2016.07.020

Chowdhury, S. and Saha, P.D. (2013). Artificial neural network (ANN) modeling of adsorption of methylene blue by NaOH-modified rice husk in a fixed-bed column system. *Environmental Science and Pollution Research 20*, 1050-1058. https://doi.org/10.1007/s11356-012-0912-2

Chowdhury, Z.Z., Zain, S.M., Rashid, A.K., Rafique, R.F. and Khalid, K. (2013). Breakthrough curve analysis for column dynamics sorption of Mn(ii) ions from wastewater by using mangostana garcinia peel-based granular-activated carbon. *Journal of Chemistry*, Article ID 959761. http://dx.doi.org/10.1155/2013/959761

Fagundez, J.L.S., Netto, M.S., Dotto, G.L. and Salau, N.P.G. (2021). A new method of developing ANN-isotherm hybrid models for the determination of thermodynamic parameters in the adsorption of ions Ag^{+}, Co^{2+} and Cu^{2+} onto zeolites ZSM-5, HY, and 4A. *Journal of Environmental Chemical Engineering 9*, 106126. https://doi.org/10.1016/j.jece.2021.106126

Fadzail, F., Hasan, M., Ibrahim, N., Mokhtar, Z., Yekti, A., Asih, P. and Syafiuddin, A. (2022). Adsorption of diclofenac sodium using low-cost activated carbon in a fixed-bed column. *Biointerface Research in Applied Chemistry 12*, 8042-8056. https://doi.org/10.33263/BRIAC126.80428056

García-González, R., Gómez-Espinosa, R.M., Ávila-Pérez, P., Garcia-Gaitán, B., García-Rivas, J.L. and Zavala-Arce, R.E. (2016). Biosorption study of Cu^{2+} onto the chitosan-cellulose cryogel. *Revista Mexicana de Ingeniería Química 15*, 311-322.

González-López, M.E., Laureano-Anzaldo, C.M., Pérez-Fonseca, A.A., Arellano, M. and Robledo-Ortiz, J.R. (2021). A discussion on linear and non-linear forms of Thomas equation for fixed-bed adsorption column modeling. *Revista Mexicana de Ingeniería Química 20*, 875-884. https://doi.org/10.24275/rmiq/Fen2337

Hernández-Abreu, A.B., Álvarez-Torrellas, S., Águeda, V.I., Larriba, M., Delgado, J.A., Calvo, P.A., García, J. (2020). New insights from modelling and estimation of mass transfer parameters in fixed-bed adsorption of bisphenol A onto carbon materials. *Journal of Contaminant Hydrology 228*, 103566. https://doi.org/10.1016/j.jconhyd.2019.103566

Hernández-Osorio, M.A., Ochoa-Velasco., C.E., García-Alvarado, M.A., Escobedo-Morales, A. and Ruiz-López, I.I. (2020). Sequential synthesis of PID controllers based on LQR method. *Revista Mexicana de Ingeniería Química 19*, 913-928. https://doi.org/10.24275/rmiq/Sim814

Konicki, W., Aleksandrzak, M., Moszýski, D. and Mijowska, E. (2017). Adsorption of anionic azo-dyes from aqueous solutions onto graphene oxide: Equilibrium, kinetic and thermodynamic studies. *Journal of Colloid and Interface Science 496*, 188-200. https://doi.org/10.1016/j.jcis.2017.02.031

Leo-Avelino, G., Urrea-Garcia, G.R., Gómez-Rodríguez, J., Pérez-Correa, S. and Aguilar-Uscanga, M.G. (2021). Natural Mexican Clinoptilolite for ethanol dehydration: adsorption-regeneration experimental parameter determination and scaling-up at pilot plant. *Revista Mexicana de Ingeniería Química 20*, Proc2358. https://doi.org/10.24275/rmiq/Proc2358

Marzban, N., Mohed, A., Filonenko, S., Hosseini, S.H., Nouri, M.J., Libra, J.A., Farru, G. (2021). Intelligent modeling and experimental study on methylene blue adsorption by sodium alginate-kaolin beads. *International Journal of Biological Macromolecules 186*, 79-91. https://doi.org/10.1016/j.ijbiomac.2021.07.006

Mendoza-Castillo, D.I., Reynel-Ávila, H.E., Sánchez-Ruiz, F.J., Trejo-Valencia, R., Jaime-Leal, J.E. and Bonilla-Petriciolet, A. (2018). Insights and pitfalls of artificial neural network modeling of competitive multi-metallic adsorption data. *Journal of Molecular Liquids 251*, 15-27. https://doi.org/10.1016/j.molliq.2017.12.030

Obón, J.M., Angosto, J.M., González-Soto, F. and Ascua, A. (2022). Prototyping a spinning adsorber submerged filter for continuous removal of wastewater contaminants. *Journal of*

Water Process Engineering 45, 102515. https://doi.org/10.1016/j.jwpe.2021.102515

Ogata, K. (2010). *Modern Control Engineering*. Fifth Edition. Prentice Hall, U.S.A.

Panis, C., Candiotto, L.Z.P., Gaboardi, S.C., Gurzenda, S., Cruz, J., Castro, M. and Lemos, B. (2022). Widespread pesticide contamination of drinking water and impact on cancer risk in Brazil. *Environmental International*, 107321. https://doi.org/10.1016/j.envint.2022.107321

Picetti, R., Deeney, M., Pastorino, S., Miller, M.R., Shah, A., Leon, D.A., Dangour, A.D. and Green, R. (2022). Nitrate and nitrite contamination in drinking water and cancer risk: A systematic review with meta-analysis. *Environmental Research 210*, 112988. https://doi.org/10.1016/j.envres.2022.112988

Promraksa, A., Siripitana, C., Rakmak, N. and Chusri, N. (2020). Modeling of supercritical CO_2 extraction of palm oil and tocopherols based on volumetric axial dispersion. *The Journal of Supercritical Fluids 166*, 105021. https://doi.org/10.1016/j.supflu.2020.105021

Qiao, J., Xiong, Y. (2021). Electrochemical oxidation technology: A review of its application in high-efficiency treatment of wastewater containing persistent organic pollutants. *Journal of Water Process Engineering 44*, 102308. https://doi.org/10.1016/j.jwpe.2021.102308

Rangabhasyiyam, S., Anu, N., Giri Nandagopal, M.S. and Selvaraju, N. (2014). Relevance of isotherm models in biosorption of pollutants by agricultural byproducts. *Journal of Environmental Chemical Engineering 2*, 398-414. https://doi.org/10.1016/j.jece.2014.01.014

Rueda-Márquez, J.J., Levchuk, I., Ibañez, P.F. and Sillanpää, M. (2020). A critical review on application of photocatalysis for toxicity reduction of real wastewaters. *Journal of Cleaner Production 258*, 120694. https://doi.org/10.1016/j.jclepro.2020.120694

Shirazi, M.M.A. and Dumeé, L.F. (2022). Membrane distillation for sustainable wastewater treatment. *Journal of Water Process Engineering 47*, 102670. https://doi.org/10.1016/j.jwpe.2022.102670

Tejeda-Tovar, C., Bonilla-Mancilla, H., Villabona-Ortiz, A., Ortega-Toro, R. and Licares-Eguavil, J. (2021a). Effect of the adsorbent dose and initial contaminant concentration on the removal of Pb(II) in a solution using *Opuntia ficus* Indica shell. *Revista Mexicana de Ingeniería Química 20*, 555-568. https://doi.org/10.24275/rmiq/IA2134

Tejeda-Tovar, C., Villabona-Ortíz, A., Ortega-Toro, R., López-Génes, J. and Negrete-Palacio, A. (2021b). Elimination of cadmium (II) in aqueous solution using corn cob (*Zea mays*) in batch system: adsorption kinetics and equilibrium. *Revista Mexicana de Ingeniería Química 20*, 1059-1077. https://doi.org/10.24275/rmiq/IA2398

Thorpe, G.R. (2022). Modelling the rate of adsorption of carbon dioxide by wheat. *Journal of Stored Products Research 97*, 101970. https://doi.org/10.1016/j.jspr.2022.101970

Torres-Ramón, E., García-Rodríguez, C.M., Estévez-Sánchez, K.H., Ruiz-López, I.I., Rodríguez-Jiménez, G.C., Romero de la Vega, G. and García-Alvarado, M.A. (2021). Optimization of a coconut oil extraction process with supercritical CO_2 considering economical and thermal variables. *The Journal of Supercritical Fluids 170*, 105160.https://doi.org/10.1016/j.supflu.2020.105160

Vargas-González, S., Núñez-Gómez, K.S., López-Sánchez, E., Tejero-Andrade, J.M., Ruiz-López, I.I. and García-Alvarado, M.A. (2021). Thermodynamic and mathematical analysis of modified Luikov's equations for simultaneous heat and mass transfer. *International Communications in Heat and Mass Transfer 120*, 105003. https://doi.org/10.1016/j.icheatmasstransfer.2020.105003

Verduzco-Navarro, I.P., Jasso-Gastinel, C.F., Rios-Donato, N., Mendizábal, E. (2020a). Red dye 40 removal by fixed-bed columns packed with alginate-chitosan sulfate hydrogels. *Revista*

Mexicana de Ingeniería Química 19, 1401-1411. https://doi.org/10.24275/rmiq/IA1123

Verduzco-Navarro, I.P., Rios-Donato, N., Jasso-Gastinel, C.F., Martínez-Gómez, A.d.J., Mendizábal, E. (2020b). Red dye 40 removal by fixed-bed columns packed with alginate-chitosan sulfate hydrogels. *Polymers 12*, 1401-1411. https://doi.org/10.3390/polym12102345

Villabona-Ortiz, A., Tejeda-Tovar, C.N. and Ortega-Toro, R. (2020). Modelling of the adsorption kinetics of chromium (VI) using waste biomaterials. *Revista Mexicana de Ingeniería Química 19*, 401-408. https://doi.org/10.24275/rmiq/IA650

Wang, Y., Wei, H., Wang, Y., Peng, C. and Dai, J. (2022). Chinese industrial water pollution and the prevention trends: An assessment based on environmental complaint reporting system (ECRS). *Alexandria Engineering Journal 60*, 5803-5812. https://doi.org/10.1016/j.aej.2021.04.015

Zhang, X. and Liu, Y. (2021). Concurrent removal of Cu(II), Co(II) and Ni(II) from wastewater by nanostructured layered sodium vanadosilicate: Competitive adsorption kinetics and mechanisms. *Journal of Environmental Chemical Engineering 9*, 105945. https://doi.org/10.1016/j.jece.2021.105945